

Semantic Disentangling Generalized Zero-Shot Learning

Zhi Chen, Ruihong Qiu, Sen Wang, Zi Huang, Jingjing Li, and Zheng Zhang

Abstract—Generalized Zero-Shot Learning (GZSL) aims to recognize images from both seen and unseen categories. Most GZSL methods typically learn to synthesize CNN visual features for the unseen classes by leveraging entire semantic information, *e.g.*, tags and attributes, and the visual features of the seen classes. Within the visual features, we define two types of features that semantic-consistent and semantic-unrelated to represent the characteristics of images annotated in attributes and less informative features of images respectively. Ideally, the semantic-unrelated information is impossible to transfer by semantic-visual relationship from seen classes to unseen classes, as the corresponding characteristics are not annotated in the semantic information. Thus, the foundation of the visual feature synthesis is not always solid as the features of the seen classes may involve semantic-unrelated information that could interfere with the alignment between semantic and visual modalities. To address this issue, in this paper, we propose a novel feature disentangling approach based on an encoder-decoder architecture to factorize visual features of images into these two latent feature spaces to extract corresponding representations. Furthermore, a relation module is incorporated into this architecture to learn semantic-visual relationship, whilst a total correlation penalty is applied to encourage the disentanglement of two latent representations. The proposed model aims to distill quality semantic-consistent representations that capture intrinsic features of seen images, which are further taken as the generation target for unseen classes. Extensive experiments conducted on seven GZSL benchmark datasets have verified the state-of-the-art performance of the proposal.

Index Terms—Generalized Zero-shot Learning, feature disentangling, variational autoencoder.

1 INTRODUCTION

HUMAN beings have an innate knowledge-acquisition ability on the textual information, where the visual appearance of an object can be naturally generated from its textual description through one’s prior visual experience and knowledge on the text-visual relationship. For example, one may have never seen a zebra in person. While given that the animal is horse-like with black and white stripes, we can imagine its appearance based on our understanding of horses, colors (*e.g.*, black, white), and texture (*e.g.*, stripes). Thus, when a zebra appears, it can be effectively identified. Such an ability is one reflection of intelligence. This scenario is also considered as an example of Zero-Shot Learning (ZSL). From the machine learning perspective, traditional supervised classification methods cannot recognize zebras if they have never been observed, due to the lack of visual training instances. It motivates the study of extending knowledge from one modality (*e.g.*, text descriptions) to another (*e.g.*, visual content), which can be naturally used in ZSL.

Generally, ZSL models [1], [2], [3], [4], [5] are developed to mimic the humans’ knowledge-acquisition ability, where the relationship between semantics and visual features will



Fig. 1: Illustration of images from 4 random classes in the AWA dataset and random 32 attributes. The annotated attributes do not cover all the discriminative characteristics among the classes.

be exploited based on the available semantic information and images of seen classes. They further learn to synthesize CNN visual features for unseen classes based on the learned semantic-visual relationship and the semantic information that is associated with unseen classes. A classifier will be trained based on both real and synthesized features for image recognition. Conventional ZSL approaches [1], [6], [7] posit that all test samples come from unseen classes, while the setting is impractical as it is hard to get prior knowledge of an object being seen or unseen in real-world applications. Generalized Zero-Shot Learning (GZSL) is extended from ZSL with a relaxed setting, where both seen and unseen images are expected to be identified through the same classifier.

Since the main challenge in GZSL is to build the con-

- Z. Chen, R. Qiu, S. Wang, Z. Huang are with the School of ITEE, University of Queensland, Brisbane, QLD 4067, Australia. E-mail: uqzichen@gmail.com, r.qiu@uq.edu.au, sen.wang@uq.edu.au, huang@itee.uq.edu.au
- J. Li is with the School of Computer Science and Engineering, University of Electronic Science and Technology of China, Chengdu 611731, China. E-mail: lijn117@yeah.net
- Zheng Zhang is with the School of Computer Science and Technology, Harbin Institute of Technology Shenzhen, Shenzhen, China. E-mail: darrenzz219@gmail.com

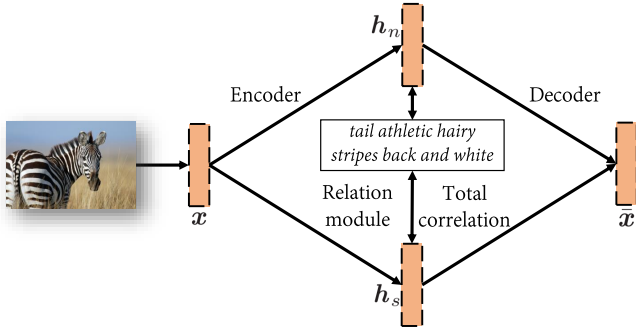


Fig. 2: Semantic-consistent h_s and semantic-unrelated h_n feature disentangling with a relation module and a total correlation penalty on top of an encoder-decoder architecture.

nection between the visual space and the semantic space, traditional GZSL methods [3], [6], [7] are embedding-based. Specifically, they either project one modality to the other, *i.e.*, visual-to-semantic/semantic-to-visual, or learn a shared latent space. To predict the class label, the semantic and visual features are used to compute the compatibility score. Thanks to the advances in generative learning, recent state-of-the-art approaches are mostly generative methods. Generative methods handle GZSL by converting it to a supervised learning problem, *i.e.*, synthesizing features for unseen samples and using them to train a classifier. The commonly used generative models for GZSL mainly include generative adversarial nets (GANs) [8], variational autoencoders (VAEs) [9], or different variants of hybrid GANs/VAEs, *e.g.*, adding a discriminator module to a VAE. The learned conditional generative model is able to generalize the intra-variance of visual features. Such a property makes the semantic-to-visual projection closer to the real data distribution. Thus, the hubness problem and the bias problem in GZSL can be alleviated [10].

However, both embedding-based and generative approaches directly leverage the visual features extracted from deep models, such as ResNet101 [11] pre-trained on ImageNet. It is worth noting that the pre-trained models are not task-specific for ZSL datasets. Thus, the CNN visual features often contain unexpected *semantic-unrelated* information, *e.g.*, background noise and features not associated with the attributes that interfere with the learning of semantic-visual alignment. As illustrated in Figure 1, AWA is an animal-specific dataset with 85 manually annotated attributes. Ideally, in the visual space, we should be able to identify the corresponding visual representations of all the semantic characteristics. However, it is impossible to annotate the attributes to cover all the semantic characteristics. For example, the ear shape is intuitively a discriminative characteristic that can be used to distinguish among animals, but it is not considered. Now that the semantic information cannot be guaranteed to be optimal, we may consider the visual space. If we can distill the part of visual features that correspond to the annotated attributes, a better alignment between visual and semantic information would be learned easily.

In this paper, we present a feature disentangling method to acquire semantic-consistent latent representations from

the original visual features for generalized zero-shot learning. As shown in Figure 2, we disentangle the underlying information of the extracted visual features into two disjoint latent representations h_s and h_n . They are learned in an encoder-decoder architecture with a relation module and a total correlation penalty. Specifically, the encoder network projects the original visual features to h_s and h_n . To make h_s coherent with the semantic embeddings, the relation module calculates a compatibility score between h_s and semantic information to guide the learning of h_s . We further apply the total correlation penalty to encourage the disentanglement between h_s and h_n . Afterward, we reconstruct the original visual features \bar{x} from the two latent representations. This reconstruction objective ensures the two latent representations to cover both semantic-consistent and semantic-unrelated information. The disentanglement component is incorporated into a conditional variational autoencoder and trained in an end-to-end manner. The proposed model is evaluated on various GZSL benchmarks and achieves state-of-the-art performance compared to the previous methods.

The main contributions of this work are summarized as follows:

- We propose a novel feature disentangling method, namely Semantic Disentangling Generalized Zero-Shot Learning (SDGZSL), to disentangle the underlying information of visual features into two latent spaces that are semantic-consistent and semantic-unrelated, respectively. The semantic-consistent representations can alleviate the performance degradation caused by the semantic-unrelated information involved in CNN visual features.
- We seamlessly incorporated the disentangling modules into a conditional variational autoencoder to learn the generation of the semantic-consistent representations.
- To facilitate the feature disentanglement of the semantic-consistent and semantic-unrelated representations, by introducing a total correlation penalty in our framework we arrive at a more accurate characterization of the annotated features.
- Extensive experiments on the widely used Attribute Pascal and Yahoo (aPaY) dataset [12], Animals with Attributes2 (AWA) dataset [6], Caltech-UCSD Birds-200-2011 (CUB) [13] dataset, and Oxford Flowers (FLO) dataset [14] show that the proposed method significantly outperforms the state-of-the-art.

2 RELATED WORK

2.1 Early Zero-shot Learning

Early solutions towards zero-shot learning can be roughly categorized as two-step methods and embedding-based methods. Pioneering works of ZSL [1], [6], [15] are designed in a two-step fashion to predict the instance labels of unseen classes. Generally, the attributes of an input instance are inferred in the first step. After that, the class label are predicted by finding the nearest class with the most similar attributes. Such a learning paradigm, especially DAP [6], has been criticized for several shortcomings [3]. (1) Even

if the predicted semantic embeddings are optimal, it is unnecessary to predict the semantic embedding as the aim of zero-shot learning is classification. (2) It is hard to extend the zero-shot learning problem to the scenario that labeled samples of unseen classes become available. (3) Alternative sources of side information (*e.g.*, textual descriptions) are not straightforward to incorporate into this learning paradigm. The following works approach zero-shot learning from the embedding perspective. ALE [3] proposes to employ embedding functions to measure the compatibility scores between a semantic embedding and a data sample. SJE [16] extends ALE by making use of structured SVM [17] and takes advantage of the structured outputs. DeVISE [18] constructs a deep visual semantic embedding model to map the 4096-dimensional visual features from AlexNet [19] to the 500 or 1000-dimensional skip-gram semantic embeddings. EZSL [20] theoretically gives the risk bound of the generalization error and connects zero-shot learning with the domain adaptation problem. More recently, SAE [5] develops a cycle embedding approach with an autoencoder to reconstruct the learned semantic embeddings into visual space. Later, the cycle architecture is also investigated in generative methods [21]. However, these early methods have not achieved satisfactory results on zero-shot learning. Recently, thanks to the advances of generative models [8], [9], by generating missing visual samples of unseen classes zero-shot learning can be converted into a supervised classification task.

2.2 Generative Zero-shot Learning

Recent state-of-the-art approaches for GZSL with generative models have achieved promising performance. Generative models can synthesize an unlimited number of visual features from side information of the unseen classes, *e.g.*, manually annotated attributes. With these synthesized features, ZSL problems become a relatively straightforward supervised classification task. The two most commonly used generative models are generative adversarial networks (GANs) [8] and variational autoencoders (VAEs) [9]. Often, both models are jointly used to form generative architectures for ZSL tasks. GAZSL [22] leverages Wasserstein GANs (WGAN) [23] to synthesize vivid visual features from noisy textual descriptions. f-CLSWGAN [24] is a similar GAN-based generative approach for ZSL, but the semantic information is based on the attributes. GDAN [25] takes a different approach with a novel structure consisting of a conditional variational autoencoder (cVAE) and a GAN that generate various visual features from class feature embeddings as input. CADA-VAE [26] leverages two aligned variational autoencoders to learn the shared latent representations between different modalities. SE-ZSL [27] adopts an autoencoder followed by an attribute regressor to train a model with three alignments: visual-to-attribute, attribute-to-visual and visual-to-attribute. The latter two feedback alignments help to improve the effectiveness of the decoder, which works as a visual feature generator. E-PGN [28] integrates the meta-learning approach into ZSL by formulating both the visual prototype generation and the class semantic inference into an adversarial framework. TF-VAEGAN [29] proposes a feedback module in a VAE-GAN model to modulate the latent representation of the generator.

However, notice that the CNN visual features contain semantic-unrelated information, *e.g.*, background noise and unannotated characteristics that may interfere with the semantic-visual alignment, we propose to factorize out the semantic-unrelated features and leverage the remaining semantic-consistent features as the generation target. The generative model we adopted in this work is a conditional variational autoencoder.

2.3 Feature Disentanglement

In most literature, disentanglement refers to independence among features of one representation [30], [31], [32], [33]. While the research community has proposed a variety of supervised [34], unsupervised [35], and semi-supervised [36] approaches to learning disentangled representations based on variational autoencoders and has devised different metrics to quantify their level of disentanglement, feature disentanglement has been rarely studied for ZSL.

Total correlation [37] is commonly used for disentanglement, most methods apply the total correlation to encourage independence among different dimensions of a representation [38]. However, in our method, it is used to isolate the dependence between the two latent representations.

There are also some unsupervised methods to distinguish between salient and irrelevant features. Contrastive principal components analysis (cPCA) [39] introduces a background dataset without the salient variance to distinguish between salient and irrelevant principal components. Based on cPCA, contrastive multivariate singular spectrum analysis (cMSSA) [40] further apply the technique on time series data and factorize into salient signals. In our paper, we also try to distinguish the salient and irrelevant features but in a supervised manner. In our work, we aim to make the salient features consistent with the semantic information, whereas the irrelevant features are irrelevant to the semantic information.

To our best knowledge, DLFZRL [41] is the only work proposed to consider feature disentanglement for ZSL. DLFZRL proposes a hierarchical disentanglement approach to learn the discriminative latent features. This approach is designed in a two-step fashion, starting with feature selection and then learning to generate the selected features. The original visual features are factorized into three latent representations, including semantic, non-semantic, and non-discriminative ones. The disentangled semantic and non-semantic visual features are used as the substitute for the original visual features. However, we argue that the non-semantic visual features do not align with the semantic embeddings. Hence it is hard to transfer the non-semantic visual features from seen to unseen classes. Moreover, our approach is trained in an end-to-end manner, which makes the generative model and the feature disentanglement module converge to a more optimal status.

3 APPROACH

This section first introduces the problem formulation and notations, then depicts the proposed approach of factorizing semantic-consistent representations for generalized zero-shot learning.

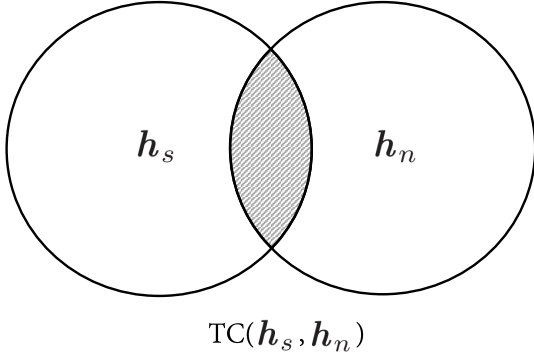


Fig. 3: The total correlation consists of all information that is shared among h_s and h_n .

3.1 Preliminaries

Let $\{\mathcal{X}^s, \mathcal{Y}^s\}$ be the dataset with S seen classes, which contains N^s training samples $\mathcal{X}^s = \{\mathbf{x}_{(i)}^s\}_{i=1}^{N^s}$ and the corresponding class labels $\mathcal{Y}^s = \{y_{(i)}^s\}_{i=1}^{N^s}$. The class labels span from 1 to S , $y^s \in \mathbf{L}^s = \{1, \dots, S\}$. Given another dataset $\{\mathcal{X}^u, \mathcal{Y}^u\}$, in which the classes are related to the seen dataset (e.g., all classes in both datasets correspond to animals). The dataset has U unseen classes and consists of N^u data instances $\mathcal{X}^u = \{\mathbf{x}_{(j)}^u\}_{j=1}^{N^u}$ with the corresponding labels $\mathcal{Y}^u = \{y_{(j)}^u\}_{j=1}^{N^u}$. The class labels are thus range from $S + 1$ to $S + U$, $y^u \in \mathbf{L}^u = \{S + 1, \dots, S + U\}$. Note that the seen and unseen classes are mutually exclusive, i.e., $\mathbf{L}^s \cap \mathbf{L}^u = \emptyset$. With respect to the semantic information $\mathcal{A} = \{\mathbf{a}_{(k)}\}_{k=1}^{S+U}$, each class from both seen and unseen is associated with a class-level semantic vector, which can be embeddings or attributes. We denote \mathcal{A}^s and \mathcal{A}^u as the semantic vectors of seen and unseen classes. In the setting of GZSL, the training instances and labels of the seen classes $\{\mathcal{X}^s, \mathcal{Y}^s\}$ and the semantic information of all classes \mathcal{A} are available during training. In the testing phase, we aim to classify the data samples $\mathbf{x}_{(j)}^u$ from the unseen classes.

Semantic-Consistent Representations. We define semantic-consistent representations h_s to represent the characteristics of images annotated in attributes. The visual features of images are extracted by a deep model, e.g., ResNet101, pre-trained on ImageNet. These visual features are not task-specific for ZSL datasets, in which the classes are usually related (e.g., they all correspond to birds). Thus, the extracted visual features may unexpectedly involve verbose information that could interfere with the semantic-visual relationship learning. The elegant solution to ZSL is attribute-based learning, which consists in introducing the intermediate space \mathcal{A} that enables the parameter sharing between classes. Ideally, if the visual features only contain information that corresponds to the annotated attributes, i.e., h_s , the visual-semantic relation can be easily learned from seen classes and further transferred to unseen classes.

Semantic-Unrelated Representations. In analogy to semantic-consistent representations, we define semantic-unrelated visual representations h_n to represent the verbose information contained in visual features which may help classification but not correspond to the annotated attributes, e.g., in Figure 1 the ear shape is an intuitively discriminative

characteristic that can help distinguish animals but does not appear in the annotated attributes.

Independence between h_s and h_n . Independence can be reflected by the mutual information, and the total correlation is one of the generalizations of the mutual information. As \mathbf{x} is factorized into h_s and h_n , all information contained within \mathbf{x} can be reflected in either h_s or h_n . In Figure 3, the shaded area is the information shared among h_s and h_n . To facilitate the independence between h_s and h_n , the total correlation can be leveraged to measure the how h_s is independent from h_n .

3.2 Feature Generation

We start by describing the generative model incorporated in our proposed framework. To model the distribution of visual features conditioned on the semantic information (labels or class-level semantic information), we leverage the conditional variational auto-encoder (cVAE) [42] as the generative model. The cVAE is a conditional directed graphical model based on the side information that modulates the prior distribution on Gaussian latent variables $\mathbf{z} \sim \mathcal{N}(\mathbf{0}, \mathbf{I})$ to generate the structured output prediction. The variational lower bound of the conditional log-likelihood in cVAE can be written as follows:

$$p_\theta(\mathbf{x}|y) \geq -KL[q_\phi(\mathbf{z}|\mathbf{x}, y)||p_\theta(\mathbf{z}|y)] + \mathbb{E}_{q_\phi(\mathbf{z}|\mathbf{x}, y)}[\log p_\theta(\mathbf{x}|\mathbf{z}, y)], \quad (1)$$

where \mathbf{x} and y denote the output vectors and the category information.

In GZSL, we aim to transfer the knowledge from seen classes to some other unseen classes. Hence, we represent the category information y in cVAE as the class embeddings \mathbf{a} to enable parameter sharing between classes. The objective function of the cVAE in our framework can then be written as:

$$\mathcal{L}_{\text{cVAE}}(\Theta; \mathbf{x}, \mathbf{a}) = -KL[q_\phi(\mathbf{z}|\mathbf{x}, \mathbf{a})||p_\theta(\mathbf{z}|\mathbf{a})] + \mathbb{E}_{q_\phi(\mathbf{z}|\mathbf{x}, \mathbf{a})}[\log p_\theta(\mathbf{x}|\mathbf{z}, \mathbf{a})], \quad (2)$$

where $\Theta = (\theta, \phi)$. The first term is the Kullback-Leibler divergence between two distributions $q_\phi(\mathbf{z}|\mathbf{x}, \mathbf{a})$ and $p_\theta(\mathbf{z}|\mathbf{a})$, whereas the second term is the reconstruction loss. As illustrated in Figure 4, we use Q_ϕ and P_θ to denote the inference and generator networks to model $q_\phi(\mathbf{z}|\mathbf{x}, \mathbf{a})$ and $p_\theta(\mathbf{z}|\mathbf{a})$, respectively. Specifically, given the real visual features \mathbf{x} and the semantic embeddings \mathbf{a} , the inference network Q_ϕ produces the latent variables \mathbf{z} . The prior of the latent variables \mathbf{z} is controlled by the class embeddings \mathbf{a} , but we can make \mathbf{z} statistically independent of \mathbf{a} , i.e., $p_\theta(\mathbf{z}|\mathbf{a}) = p_\theta(\mathbf{z})$ [43]. The generator network P_ϕ leverages the inferred latent variables \mathbf{z} and the class embeddings \mathbf{a} to reconstruct the visual features $\hat{\mathbf{x}}$.

3.3 Feature Disentanglement

While the cVAE learned in Equation 2 can generate sub-par visual features for unseen classes based on the semantic embeddings, it contains semantic-unrelated information that is detrimental for knowledge transferring from seen to unseen classes.

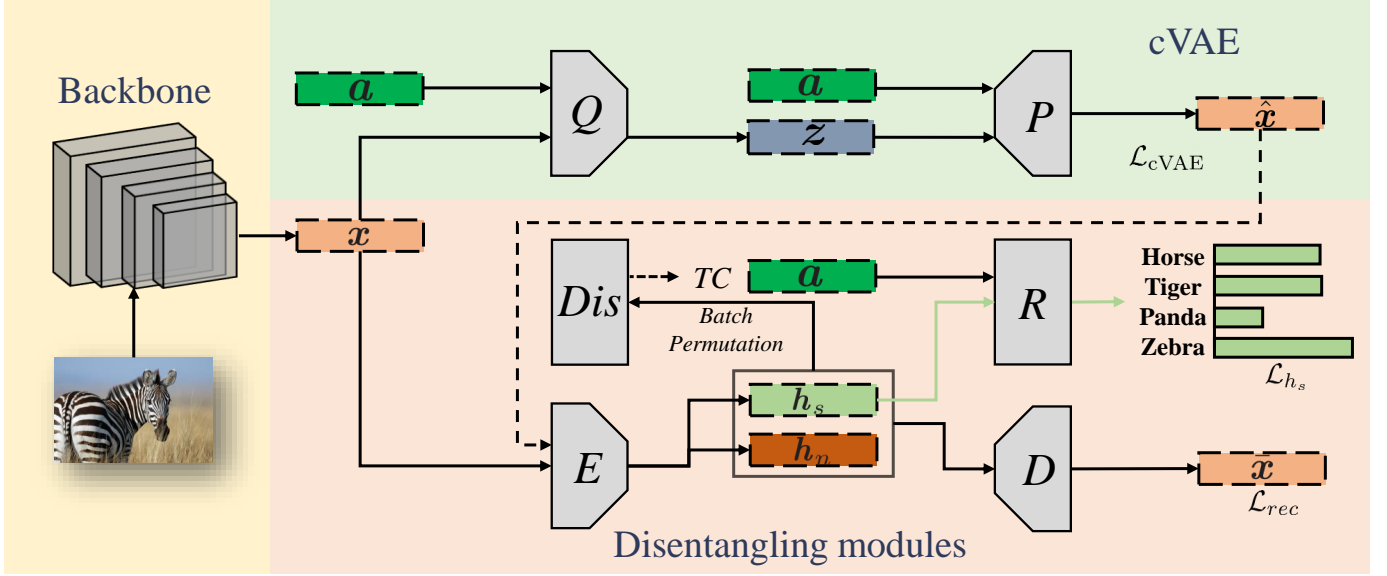


Fig. 4: An illustration of our proposed SDGZSL. Apart from the backbone that extracts visual features \mathbf{x} from an image, the overall framework consists of two major parts: (i) a CVAE model for generating visual features; (ii) disentangling modules to learn two disjoint latent representations. The inference network Q takes visual feature \mathbf{x} and the semantic embedding \mathbf{a} of the corresponding class to infer a latent variable \mathbf{z} , which is further used by generative network P to generate/reconstruct the visual features $\hat{\mathbf{x}}$ conditioned on the semantic embedding \mathbf{a} . In the disentangling modules, an encoder E projects both the original \mathbf{x} and the generated visual features $\hat{\mathbf{x}}$ into the latent representation \mathbf{h} , and it is disentangled into semantic-consistent \mathbf{h}_s and semantic-unrelated \mathbf{h}_n representations. \mathbf{h}_s are concatenated with random semantic vectors \mathbf{a} and calculate the compatibility score with the relation module R , so that \mathbf{h}_s is optimized to be consistent with semantic information. A total correlation penalty is applied on \mathbf{h}_s and \mathbf{h}_n to encourage disentanglement. \mathbf{h}_s and \mathbf{h}_n are then used to reconstruct visual features $\bar{\mathbf{x}}$ with the reconstruction loss function \mathcal{L}_{rec} .

The overall architecture of the proposed semantic disentangling framework is illustrated in Figure 4. First of all, the visual features of images are extracted from the ResNet101 model, which is pre-trained on the ImageNet dataset. We argue that these visual features may contain semantic-unrelated information, *e.g.*, background noise and features not associated with the annotated attributes. It is worth noting that, in GZSL, the core mission is to transfer the semantic-visual relationship from seen classes to unseen classes. However, as these visual concepts of the semantic-unrelated information are not consistent with the manually annotated semantic information, it is intuitively hard to align the relationship from semantic space to visual space and further transfer to unseen classes. Thus, we aim to disentangle the visual features into two disjoint subspaces, which are semantic-consistent and semantic-unrelated, and discard the semantic-unrelated representations.

The disentangling modules are developed with an encoder-decoder architecture, coupled with a relation module and a total correlation penalty. The relation module and the total correlation penalty will be elucidated in the next sub-sections. An encoder E_ψ parameterized with ψ is adopted to map a visual feature vector $\mathbf{x}_{(i)}$ to a latent representation $\mathbf{h}_{(i)}$, *i.e.*, $E_\psi: \mathbb{R}^d \rightarrow \mathbb{R}^{l+m}$, where l and m are the number of dimensions of the semantic-consistent and semantic-unrelated representations. Then, following Python slice notation we have:

$$\mathbf{h}_s = \mathbf{h}_{[0:l]}, \quad \mathbf{h}_n = \mathbf{h}_{[l:l+m]}, \quad (3)$$

where \mathbf{h}_s and \mathbf{h}_n denote semantic-consistent and semantic-unrelated representations, respectively. A decoder D_ω parameterized with ω should be able to map the two latent representations back to the original visual feature vector, *i.e.*, $D_\omega: \mathbb{R}^{l+m} \rightarrow \mathbb{R}^d$. We denote the reconstructed visual features as $\hat{\mathbf{x}}_{(i)}$. Thus, the two latent representations are optimized to preserve the information of the visual features. The reconstruction objective can be formulated as:

$$\begin{aligned} \mathcal{L}_{rec} &= \sum_i \|\mathbf{x}_{(i)} - \hat{\mathbf{x}}_{(i)}\|^2 \\ &= \sum_i \|\mathbf{x}_{(i)} - D(\mathbf{h}_{s(i)}, \mathbf{h}_{n(i)})\|^2, \end{aligned} \quad (4)$$

where we calculate the mean squared error between the original visual features \mathbf{x} and the reconstructed visual features $\bar{\mathbf{x}}$.

3.4 Learning Semantic-visual Relationship

With the encoder-decoder architecture, we constrain the latent representation \mathbf{h} to preserve both the semantic-consistent and the semantic-unrelated features from visual features. Afterward, we aim to make \mathbf{h}_s contain the semantic-consistent information. A relation module is adopted to learn the semantic-consistent representations by maximizing the compatibility score between a latent representation $\mathbf{h}_{s(i)}$ and the corresponding semantic embeddings $\mathbf{a}_{(k)}^s$. Our relation module is similar to Relation Network (RN) [44], which is a meta-learning approach for few-shot learning. Unlike other few-shot learning approaches that

learn a fixed manually defined similarity metric or a linear classifier between the image samples and queries, RN provides a self-adaptive similarity metric to the data.

The relation module R_κ parameterized with κ learns the pair-wise relationship between the latent representations and random semantic vectors. The input of R is the pairs of a latent representation \mathbf{h}_s and N^c unique semantic embeddings $\mathcal{A}^{batch} = \{\mathbf{a}_{(c)}\}_{c=1}^{N^c}$ from a training batch with B training instances. The ground-truth compatibility score of the matched pairs is set to be 1; the mismatched pairs are 0, which can be formulated as:

$$cmp(\mathbf{h}_{(t)}, \mathbf{a}_{(c)}) = \begin{cases} 0, & y_{(t)} \neq y_{(c)} \\ 1, & y_{(t)} = y_{(c)} \end{cases}, \quad (5)$$

where t and c refer to the t -th semantic-consistent representation and c -th unique semantic embedding in a training batch, $y_{(t)}$ and $y_{(c)}$ denote the class label of $\mathbf{h}_{(t)}$ and $\mathbf{a}_{(c)}$.

With the compatibility scores in Equation 5, we now formulate the loss function for the semantics embeddings \mathcal{A}^{batch} and semantic-consistent information. We propose to use the relation module R_κ with a Sigmoid activation function that outputs the learned compatibility score between 0 and 1 for each pair. The loss function for optimizing \mathbf{h}_s can then be formulated as:

$$\mathcal{L}_{\mathbf{h}_s} = \sum_t^B \sum_c^{N^c} \|R_\kappa(\mathbf{h}_{st}, \mathbf{a}_c) - cmp(\mathbf{h}_{st}, \mathbf{a}_c)\|^2 \quad (6)$$

where we calculate the mean squared error between the output compatibility score of each pair of \mathbf{h}_s and \mathbf{a}_c and the ground-truth in every single training batch. Normally, we have $N^c \leq B$ as the sampled visual feature vectors in one batch may contain multiple ones from the same class.

3.5 Total Correlation Penalty

To encourage the disentanglement between semantic-consistent \mathbf{h}_s and semantic-unrelated \mathbf{h}_n representations, we introduce a *total correlation* penalty in our proposed method. Total Correlation [37] is a measurement of dependence for multiple random variables. In information theory, total correlation is one of many generalizations of mutual information to random variables. It has been a key component in recent methods towards disentanglement. FactorVAE [38] is proposed to disentangle by making the distribution of representations to be factorial and thus achieves independence across dimensions. Specifically, independence among dimensions is achieved by applying the total correlation penalty on an original representation and its random permuted representation across dimensions. In our paper, we aim to achieve independence between two representations rather than dimensions.

Within the encoding procedure, the latent representation $\mathbf{h} \sim \gamma(\mathbf{h} | \mathbf{x})$ is expected to contain both the semantic and the non-semantic information. Therefore, the disentanglement between these two streams of information is crucial for meaningful representation learning. As the relation module can facilitate the semantic-consistent representation \mathbf{h}_s learning, we aim to make \mathbf{h}_n semantic-unrelated by encouraging the disentanglement between \mathbf{h}_n and \mathbf{h}_s . In this paper, the desired disentangle property of the latent representation \mathbf{h} is different from that in FactorVAE. We only

want to disentangle \mathbf{h}_s and \mathbf{h}_n to represent the semantic-consistent and the semantic-unrelated information. From a probabilistic point of view, we can think of both of them come from a different conditional distribution:

$$\mathbf{h}_s \sim \gamma_1(\mathbf{h}_s | \mathbf{x}), \quad \mathbf{h}_n \sim \gamma_2(\mathbf{h}_n | \mathbf{x}). \quad (7)$$

Hence, for the two latent representations, the total correlation can be formulated as

$$TC = \text{KL}(\gamma || \gamma_1 \cdot \gamma_2), \quad (8)$$

where $\gamma := \gamma(\mathbf{h}_s, \mathbf{h}_n | \mathbf{x})$ is the joint conditional probability of \mathbf{h}_s and \mathbf{h}_n . As the two representations can be seen as a real one and a fake one, we apply the density ratio trick to compute efficiently in an adversarial manner. A discriminator Dis_φ parameterized with φ can be built on top of the model, which outputs an estimate of the probability $Dis_\varphi(\mathbf{h}_s)$ that its input is independent. Thus,

$$TC = \mathbb{E}_\gamma \left(\log \frac{\gamma}{\gamma_1 \cdot \gamma_2} \right)$$

where the density ratio of the total correlation term is:

$$r(\mathbf{h}) = \frac{\gamma}{\gamma_1 \cdot \gamma_2}. \quad (9)$$

Let γ_3 denote $\gamma_1 \cdot \gamma_2$. Assume there are equal numbers of in/dependent pairs of \mathbf{h}_s and \mathbf{h}_n , when $y = 1$, \mathbf{h}_s and \mathbf{h}_n inter-dependent, and when $y = 0$, \mathbf{h}_s and \mathbf{h}_n are independent. We have

$$r(\mathbf{h}) = \frac{\gamma}{\gamma_1 \cdot \gamma_2} \quad (10)$$

$$= \frac{\gamma}{\gamma_3} \quad (11)$$

$$= \frac{\tau(\mathbf{h} | y = 1)}{\tau(\mathbf{h} | y = 0)} \quad (12)$$

$$= \frac{\tau(y = 1 | \mathbf{h})\tau(\mathbf{h})/\tau(y = 1)}{\tau(y = 0 | \mathbf{h})\tau(\mathbf{h})/\tau(y = 0)} \quad (13)$$

$$= \frac{\tau(y = 1 | \mathbf{h})}{\tau(y = 0 | \mathbf{h})} \quad (14)$$

$$= \frac{\tau(y = 1 | \mathbf{h})}{1 - \tau(y = 1 | \mathbf{h})}. \quad (15)$$

If we use a classifier/discriminator $Dis_\varphi(\mathbf{h})$ to represent the term $\tau(y = 1 | \mathbf{h})$, we can approximate the density ratio above as:

$$r(\mathbf{h}) \approx \frac{Dis_\varphi(\mathbf{h})}{1 - Dis_\varphi(\mathbf{h})}. \quad (16)$$

Thus, the total correlation can be approximated by:

$$TC \approx \mathbb{E}_\gamma \left(\log \frac{Dis_\varphi(\mathbf{h})}{1 - Dis_\varphi(\mathbf{h})} \right), \quad (17)$$

Simultaneously, we train the discriminator Dis_φ to maximize the probability of assigning the correct label to both \mathbf{h} and $\tilde{\mathbf{h}}$:

$$\mathcal{L}_{dis} = \log Dis_\varphi(\mathbf{h}) + \log(1 - Dis_\varphi(\tilde{\mathbf{h}})), \quad (18)$$

where $\tilde{\mathbf{h}}$ is the result by randomly permuting each \mathbf{h}_s and \mathbf{h}_n across the batch.

The permutation process is described as following: (1) Given a batch of latent representations $\{\mathbf{h}_{(t)}\}_{t=1}^B$; (2) they are split into $\{\mathbf{h}_{s(t)}\}_{t=1}^B$ and $\{\mathbf{h}_{n(t)}\}_{t=1}^B$; (3) for both \mathbf{h}_s and \mathbf{h}_n , we randomly permute the batch indexes twice on $\mathcal{B} = \{1, \dots, B\}$, yielding \mathcal{B}' and \mathcal{B}'' ; (4) with the permuted indexes, reorder the latent representations $\{\mathbf{h}_{s\mathcal{B}'(t)}\}_{t=1}^B$, $\{\mathbf{h}_{n\mathcal{B}''(t)}\}_{t=1}^B$ and concatenate them into $\{\tilde{\mathbf{h}}_{(t)}\}_{t=1}^B$.

3.6 Training and Inference

We now introduce the training and generalized zero-shot learning inference in our framework. As illustrated in Figure 4, the cVAE model is seamlessly incorporated into our feature disentangling components so that the framework can be trained in an end-to-end manner. The adversarial network is generally known as hard to train, especially with a bunch of network modules. Algorithm 1 shows the pseudo code of the model training. We iteratively train the Dis_φ together with the overall framework for n_{dis} steps and then fix the weights in Dis_φ to train other components. In Algorithm 1, the weights for $\mathcal{L}_{\mathbf{h}_s}$, TC , and \mathcal{L}_{dis} are denoted as λ_1, λ_2 and λ_3 , respectively.

Once the training of SDGZSL is converged, the semantic-consistent representations $\bar{\mathbf{h}}_s^u$ of unseen classes can be generated by the generative network P_θ and disentangling encoder E_ψ from the Gaussian noise \mathbf{z} and the unseen semantic embeddings \mathbf{a}^u , i.e., $P_\theta : \mathbb{R}^z \times \mathbb{R}^k \rightarrow \mathbb{R}^d$, $E_\psi : \mathbb{R}^d \rightarrow \mathbb{R}^{l+m}$. \mathbf{z} represents the dimensions of the latent variables \mathbf{z} . Then, we disentangle the training seen features $\{\mathbf{x}_{s(i)}^s\}_{i=1}^{N^s}$ into $\{\mathbf{h}_{s(i)}^s\}_{i=1}^{N^s}$, together with the generated unseen semantic-consistent representations $\bar{\mathbf{h}}_s^u$ we can simply train a supervised classifier. Further prediction for either seen or unseen objects can be conducted by supervised classification. In our paper, a simple softmax classifier is adopted to evaluate the GZSL performance.

Algorithm 1 SDGZSL training

Input: $\{\mathcal{X}^s, \mathcal{Y}^s\}$ and \mathcal{A}^s

Initialize: φ and $W = \{\phi, \theta, \psi, \omega, \kappa\}$

- 1: **while** not converged **do**
 - 2: Randomly select a batch $\{\mathbf{x}_{(t)}^s, \mathbf{y}_{(t)}^s\}_{t=1}^B, \{\mathbf{a}_{(c)}^s\}_{c=1}^{N^c}$
 - 3: **for** step = 0, ..., n_{dis} **do**
 - 4: Compute $\tilde{\mathbf{h}}$ and \mathbf{h} with ϕ, θ, ψ
 - 5: Vector permutation for $\tilde{\mathbf{h}}$ and \mathbf{h}
 - 6: Compute $\lambda_3 \mathcal{L}_{dis}$
 - 7: Update $\varphi \leftarrow \varphi + \lambda \nabla_\varphi \mathcal{L}_{dis}$
 - 8: Compute $\mathcal{L}_{overall} = \mathcal{L}_{cVAE} + \mathcal{L}_{rec} + \lambda_1 \mathcal{L}_{\mathbf{h}_s}$
 - 9: Update $W \leftarrow W + \lambda \nabla_W \mathcal{L}_{overall}$
 - 10: **end for**
 - 11: Randomly select a batch $\{\mathbf{x}_{(t)}^s, \mathbf{y}_{(t)}^s\}_{t=1}^B, \{\mathbf{a}_{(c)}^s\}_{c=1}^{N^c}$
 - 12: Compute $\mathcal{L}_{overall} = \lambda_2 TC + \mathcal{L}_{cVAE} + \mathcal{L}_{rec} + \lambda_1 \mathcal{L}_{\mathbf{h}_s}$
 - 13: Update $W \leftarrow W + \lambda \nabla_W \mathcal{L}_{overall}$
 - 14: **end while**
-

Output trained generative network P_θ and encoder E_ψ

TABLE 1: Statistics of the four zero-shot learning datasets.

Dataset	aPaY	AWA	CUB	FLO
# of Attributes	64	85	1024	1024
# of Seen Classes	20	40	150	82
# of Unseen Classes	12	10	50	20
# of Total Images	18,627	30,475	11,788	8,189

4 EXPERIMENTS

In this section, we conduct experiments on four standard zero-shot learning benchmarks to evaluate the effectiveness of the proposed model.

4.1 Experimental Setting

4.1.1 Datasets

The proposed framework is evaluated on widely used benchmark datasets of image classification, including two coarse-grained datasets (Attribute Pascal and Yahoo (aPaY) [12] and Animals with Attributes2 (AWA) [6]) and two fine-grained datasets (Caltech-UCSD Birds-200-2011 (CUB) [13] and Oxford Flowers (FLO) [14]). aPaY contains 18,627 images from 42 classes and is annotated with 64 attributes. It combines datasets a-Pascal and a-Yahoo, which has 30 and 12 classes respectively. a-Yahoo dataset collects images from Yahoo image search engine to supplement a-Pascal dataset. The categories in the a-Yahoo dataset are chosen to be similar to a-Pascal, e.g., "wolf" and "dog". AWA is a relatively larger coarse-grained dataset with 30,475 images from 50 animal species, in which 40 species are selected as seen classes and the rest as unseen classes. Each species in the dataset is annotated with 85 attributes. CUB consists of 11,788 images from fine-grained bird species with 150 seen and 50 unseen classes. FLO contains 102 flower categories with 82 seen and 20 unseen classes. The semantic embeddings of FLO and CUB are 1,024-dimensional character-based CNN-RNN features [52] extracted from the fine-grained visual descriptions (10 sentences per image). Following [53] and [14], the standard dataset splits are adopted and the statistics of the four datasets are shown in Table 1.

4.1.2 Evaluation Protocol

Early ZSL comparison [54] adopts per-image accuracy as the evaluation protocol, which calculates the percentage of image predictions that are made correctly. However, this evaluation protocol has been criticized for leading unfair results on those highly populated classes [53]. Therefore, our evaluation is based on per-class accuracy, which average the accuracies from all test classes. Specifically, we use per-class accuracy to calculate the accuracy for U and S as shown in Table 2, which means classifying unseen test samples and seen test samples over all seen and unseen classes, respectively. The metric used to evaluate the GZSL task is harmonic mean, which computes the joint accuracy of the seen and unseen classes. The formula used to calculate the harmonic mean H can be written as:

$$H = \frac{(2 \times U \times S)}{(U + S)}, \quad (19)$$

TABLE 2: GZSL accuracy (%) on five datasets. We report the accuracies of unseen, seen classes and their harmonic mean, which are denoted as U, S and H. The best results of the harmonic mean are formatted in bold. † and ‡ represent embedding-based and generative methods, respectively.

	Methods	aPaY			AWA			CUB			FLO		
		U	S	H	U	S	H	U	S	H	U	S	H
†	LFGAA [45]	-	-	-	27.0	93.4	41.9	36.2	80.9	50.0	-	-	-
	DCN [46]	14.2	75.0	23.9	25.5	84.2	39.1	28.4	60.7	38.7	-	-	-
	TCN [47]	24.1	64.0	35.1	61.2	65.8	63.4	52.6	52.0	52.3	-	-	-
	DVBE [48]	32.6	58.3	41.8	63.6	70.8	67.0	53.2	60.2	56.5	-	-	-
‡	GAZSL [22]	14.2	78.6	24.0	35.4	86.9	50.3	31.7	61.3	41.8	28.1	77.4	41.2
	f-CLSWGAN [24]	32.9	61.7	42.9	56.1	65.5	60.4	43.7	57.7	49.7	59.0	73.8	65.6
	cycle-CLSWGAN [49]	-	-	-	56.9	64.0	60.2	45.7	61.0	52.3	59.2	72.5	65.1
	CADA-VAE [26]	31.7	55.1	40.3	55.8	75.0	63.9	51.6	53.5	52.4	51.6	75.6	61.3
	f-VAEGAN-D2 [50]	-	-	-	57.6	70.6	63.5	48.4	60.1	53.6	56.8	74.9	64.6
	DLFZRL [41]	-	-	38.5	-	-	60.9	-	-	51.9	-	-	-
	TF-VAEGAN [29]	-	-	-	59.8	75.1	66.6	52.8	64.7	58.1	62.5	84.1	71.7
	OCD-CVAE [51]	-	-	-	59.5	73.4	65.7	44.8	59.9	51.3	-	-	-
	E-PGN [28]	-	-	-	52.6	83.5	64.6	52.0	61.1	56.2	71.5	82.2	76.5
	SDGZSL	38.0	57.4	45.7	64.6	73.6	68.8	59.9	66.4	63.0	83.3	90.2	86.6

where U and S denote the average per-class top-1 accuracy of unseen and seen classes, respectively. A high harmonic mean indicates the good performance of both seen and unseen classes.

4.1.3 Implementation

Our framework is implemented by the popular deep learning framework PyTorch 1.4. The disentangling encoder E_ψ and decoder D_ω contain one and two fully connected (FC) layers, respectively. Each layer is followed a LeakyReLU activation function layer and a dropout layer. The numbers of hidden units of E_ψ and D_ω are $[l + m]$ and $[2048, 2048]$, where l and m are the numbers of dimensions of \mathbf{h}_s and \mathbf{h}_n . The relation module R_κ is built with two FC layers, where the first layers is followed by a ReLU activation function layer and the second layer is followed by a Sigmoid activation function layer. The discriminator is implemented with a single FC layer followed by a Sigmoid activation function layer. We set the dimension number l and m as the same value between 64 and 512. The hyper-parameters for relation weight λ_1 , TC weight λ_2 , and discriminator loss λ_3 as between 0.1 and 5. The optimal values for each dataset can be found in Section 4.4.3. We use Adam optimizer with $\beta_1 = 0.9$, $\beta_2 = 0.999$ and batch size with 64. For the generative model cVAE, we use a five-layer MLP for encoder Q_ϕ and its structure can be written as: FC-LeakyReLU-FC-Dropout-LeakyReLU-FC for the first part; a single FC layer for the mean vector output; FC-Dropout-Softplus for the variance vector output. Another three-layer MLP for decoder P_θ can be written as: FC-ReLU-Dropout-FC-LeakyReLU. We warm up the KL term and the TC term gradually with increasing epochs. All the experiments are performed on a workstation with two NVIDIA GeForce GTX 2080 Ti GPUs.

4.2 Comparison With State-of-the-art Methods

Table 2 shows the GZSL performance of compared methods and ours. We choose the state-of-the-art embedding-based

and generative methods over the past three years. They are marked with † and ‡ respectively.

Compared Methods. The pioneering generative zero-shot learning methods GAZSL [22] and f-CLSWGAN [24] leverage a conditional wasserstein GAN (cWGAN) to generate synthetic visual features and convert zero-shot learning into a supervised classification problem. cycle-CLSWGAN [49] couples f-CLSWGAN with a reverse generative model and further enforce the cycle-consistent conditional generation between semantic and visual spaces. CADA-VAE [26] learns to generate modality-invariant features by developing a dual VAE model and sharing the two latent spaces of VAEs. f-VAEGAN-D2 [50] proposes a hybrid model by combining the strength of VAE and GANs. DLFZRL [41] studies the feature disentanglement for zero-shot learning and proposes to factorize the CNN features into several parts. TF-VAEGAN [29] leverages a feedback module to improve f-VAEGAN-D2. OCD-CVAE [51] learns to generate hard samples to mimic the distribution on class level. E-PGN [28] applies meta-learning approach to episodically learn the visual prototypes for unseen classes. Unlike the early embedding-based methods that can achieve poor performance only on generalized zero-shot learning, the recent embedding-based methods are competitive to the generative zero-shot learning approaches. LFGAA [45] proposes to progressively embed the latent feature with attribute attention mechanism. DCN [46] considers uncertainty calibration for generalized zero-shot learning by calibrating the entropy on unseen classes. TCN [47] leverages a simple yet effective contrastive model to transfer the discriminative property to unseen classes. DVBE [48] constructs two complementary visual representations to approach seen and unseen domains respectively. Here, we directly report the highest performance of the compared methods from the corresponding papers.

Analysis on the Results. Generally, our proposed method consistently outperforms all the compared methods. All these methods directly use the visual features extracted from a pre-trained ResNet101 model, which limits semantic-

TABLE 3: GZSL accuracy (%) comparison with traditional methods on four datasets. We report the accuracies of unseen, seen classes and their harmonic mean, which are denoted as U, S and H. The best results of the harmonic mean are formatted in bold.

Methods	aPaY			AWA			CUB			FLO		
	U	S	H	U	S	H	U	S	H	U	S	H
DAP [6]	4.8	78.3	9.0	0.9	84.7	0.0	1.7	67.9	3.3	-	-	-
CONSE [1]	0.0	91.2	0.0	0.5	90.6	1.0	2.0	70.6	3.9	-	-	-
LATEM [2]	0.1	73.0	0.2	13.3	77.3	20.0	15.2	57.3	24.0	6.6	47.6	11.5
ALE [3]	4.6	73.7	8.7	14.0	81.8	23.9	23.7	62.8	34.4	13.3	61.6	21.9
DeVise [18]	3.5	78.4	6.7	17.1	74.7	27.8	23.8	53.0	32.8	13.2	82.6	22.8
SJE [16]	1.3	71.4	2.6	8.0	73.9	14.4	23.5	59.2	33.6	-	-	-
ESZSL [20]	2.4	70.1	4.6	5.9	77.8	11.0	14.7	56.5	23.3	-	-	-
SYNC [4]	7.4	66.3	13.3	9.7	89.7	17.5	11.5	70.9	19.8	-	-	-
SAE [5]	0.4	80.9	0.9	1.1	82.2	2.2	7.8	54.0	13.6	-	-	-
SDGZSL	11.1	71.8	19.3	21.4	88.1	34.4	25.6	63.4	36.5	24.8	80.0	37.9

visual alignment learning. GAZSL and f-CLSWGAN can achieve significantly better performance than traditional embedding-based methods as the generated unseen samples can essentially solve the most two common issues in GZSL, *i.e.*, hubness and bias [10]. However, the proposed generative model is not specifically designed for GZSL. The following methods improve the generative models by incorporating specific techniques for GZSL. The intuition of this work is in agreement with DLFZRL [41], we both aim to disentangle more effective representations from visual features. DLFZRL proposes to disentangle the discriminative features from visual features, both semantic and non-semantic. However, we argue that the non-semantic discriminative features cannot be transferred from seen classes to unseen classes. The conditional generative models learn to project the semantic vectors to the visual space, but intuitively there is no way to generalize the non-semantic discriminative features from the semantic perspective. As can be seen from the performance comparison, our method surpasses DLFZRL on all the datasets. Our method is also applicable to the generative methods mentioned above. It is worth mentioning that unlike DFLZRL that is designed in a two-stage process, we carefully design our framework by incorporating the disentangling modules into the generative model so that the overall framework can be trained in an end-to-end manner.

4.3 Comparison with Traditional Methods

To further demonstrate the superiority of the disentangled semantic-consistent representations, we conduct experiments on traditional embeddings methods. Specifically, we use the converged encoder E_{ψ} to process the original visual features. The yielded semantic-consistent representations h_s substitute the original visual features to learn a compatibility function. We choose the standard embeddings method ALE [3] as the base method. Table 3 shows the performance comparison between our approach and the most representative traditional embedding-based approaches. We present their performance that are reported in [53]. It can be seen from the table that traditional embedding-based methods perform poorly on GZSL setting, especially on unseen classes. These traditional embedding-based methods

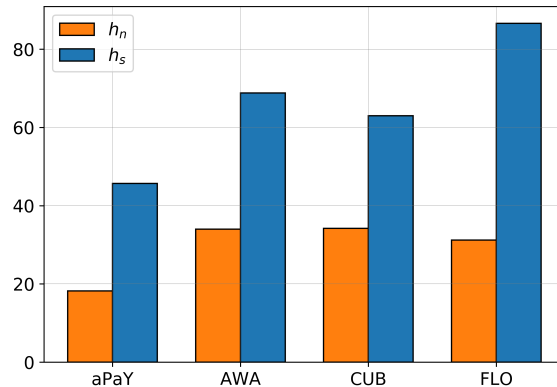


Fig. 5: GZSL accuracy (in %) comparison between h_s and h_n .

are originally proposed for conventional zero-shot learning setting that only aims to classify test unseen samples over unseen classes. We argue that the simple embeddings functions cannot draw a clear distinction between the seen class domain and the unseen class domain so that under GZSL setting the unseen class samples tend to be misclassified into seen classes. However, our semantic-consistent representations can alleviate this problem. From the performance table, training with our semantic-consistent representations instead of the original visual features, ALE can boost the performance by a large margin. The improvement verifies the semantic-consistent representations can help to transfer visual-semantic relationship from seen classes to unseen classes.

4.4 Model Analysis

4.4.1 Ablation Study

In this ablation study, we evaluate various stripped-down versions of our full proposed model to validate the contributions of the key disentangling components of the model. In Table 4, we report the GZSL performance of each version on the four benchmark datasets.

TABLE 4: Ablation Study GZSL accuracy (%) on five datasets. U, S and H represent unseen, seen and harmonic mean, respectively. The best results of harmonic mean are formatted in bold.

Settings	aPaY			AWA			CUB			FLO		
	U	S	H	U	S	H	U	S	H	U	S	H
cVAE	30.2	55.3	39.0	54.4	72.6	62.2	47.0	59.9	52.7	60.1	89.6	71.9
SDGZSL w/o RN&TC	14.6	37.0	21.0	41.3	70.0	51.9	25.1	54.7	34.5	56.6	87.6	68.7
SDGZSL w/o TC	33.8	49.1	40.0	45.7	79.4	58.0	23.6	46.2	31.2	44.8	65.7	53.3
SDGZSL w/o RN	27.3	41.9	33.1	48.5	64.6	55.5	20.8	31.4	25.0	40.6	67.6	50.7
SDGZSL	38.0	57.4	45.7	64.6	73.6	68.8	59.9	66.4	63.0	83.3	90.2	86.6

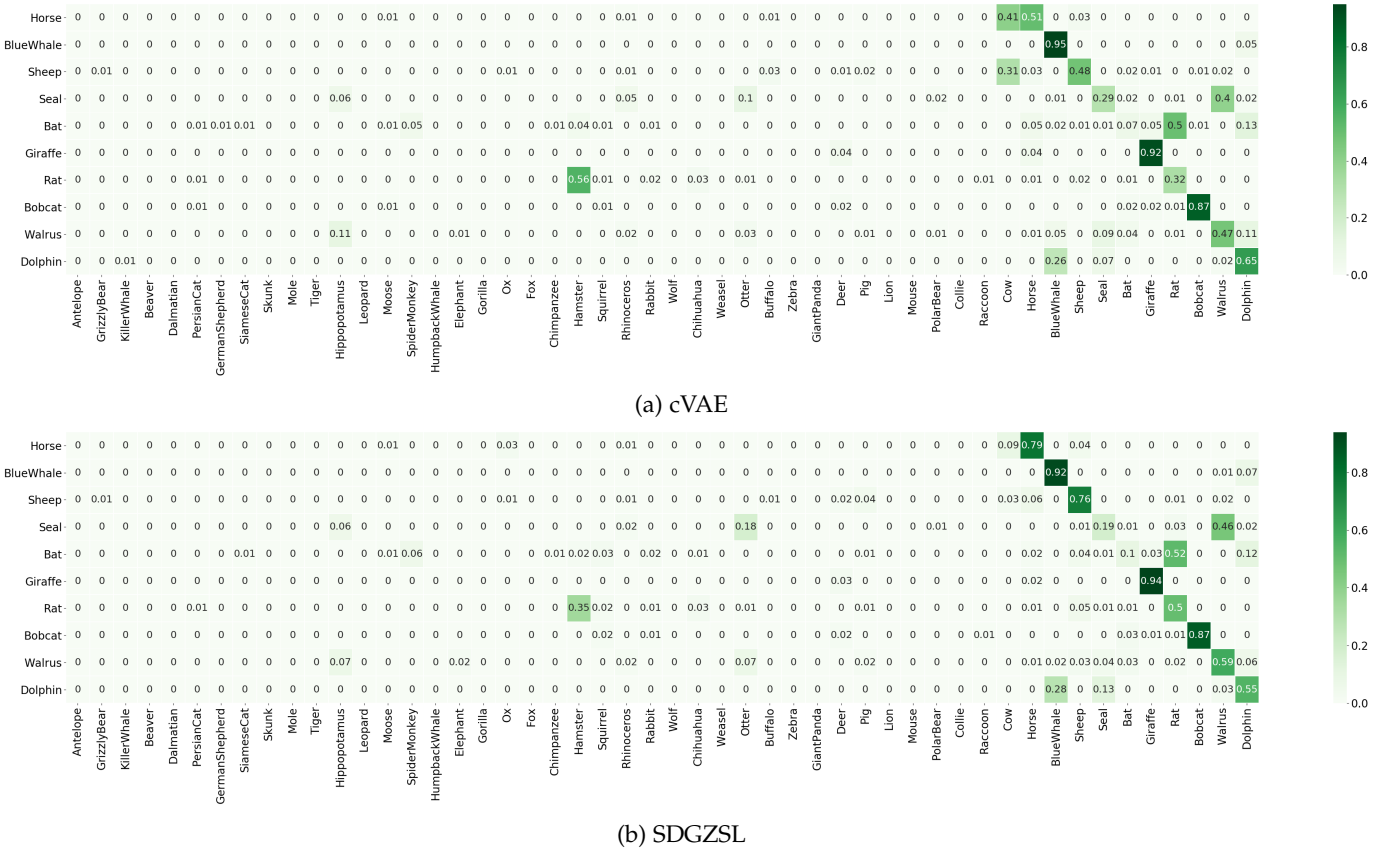


Fig. 6: The comparison between cVAE and the proposed method on confusion matrices of the unseen images being predicted over all classes. The vertical axis denotes the ground truth and the horizontal axis represents the predictions.

cVAE represents the base conditional generative model adopted in our proposed method, in which we do not apply our feature disentangling components. The generation target is the original visual features extracted from the ResNet101 model. It can achieve results similar to the compared methods that use a simple generative model, e.g., GAN or cVAE. In our cVAE implementation, by carefully design the layers and activation functions the performance of our cVAE is competitive to other state-of-the-art methods. As the generative model is not the key component in our proposed method, we do not provide further discussion about the design of the cVAE.

SDGZSL w/o RN&TC is the cVAE setting with our encoder-decoder model alone. Since there is no constraint in the latent space, the semantic information is randomly separated into h_s and h_n so that h_s loses significant information

of the visual features. This experimental setting further demonstrates that the performance improvement does not come from the simple dimension reduction technique by using an autoencoder.

SDGZSL w/o TC represents our full method without the total correlation penalty, i.e., the encoder-decoder model coupled with the relation module. The performance is still comparatively poor, but significantly better than SDGZSL w/o RN&TC as the relation module starts to help h_s again more semantic information. However, without total correlation penalty, the entanglement between h_s and h_n degrades the performance. SDGZSL w/o RN denotes the setting without the relation module, it can be seen the performance is unsatisfactory. Without the semantic-visual relationship learning from the relation module, the information in the latent space cannot be explicitly allocated to h_s and h_n .

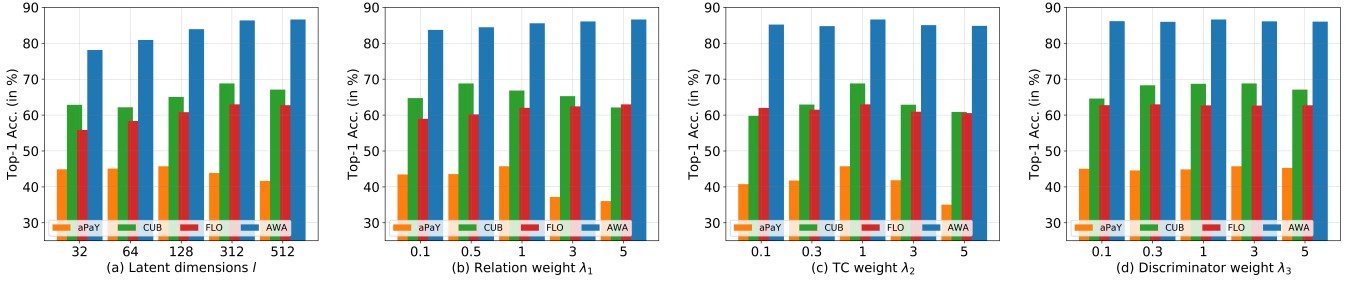


Fig. 7: (a) - (d): Hyper-parameter analysis for latent dimensions l , relation weight λ_1 , TC weight λ_2 and discriminator weight λ_3 . They represent the latent dimensions, the weights for the visual-semantic interaction, the total correlation and the regularization term.

Thus, the disentanglement cannot be achieved with respect to the semantics.

We also provide quantitative analysis on the latent representations. In Figure 5, we show the performance comparison between h_s and h_n . Our goal aims to make the h_s capable of being consistent with semantics, but we are curious about the result of training the classification model with h_n . It can be seen that h_s can achieve significantly better performance than h_n . As h_n is unrelated to semantic information, it is hard to transfer the connection between semantic to semantic-unrelated representations from seen to unseen classes. In summary, all the components in our proposed model significantly contribute to the full model.

4.4.2 Class-wise Analysis

To validate the merit for specific classes from our disentanglement approach, we compare the class-wise performance of unseen classes in AWA between the base generative method, *i.e.*, a standard cVAE, and the proposed SDGZSL. As shown in Figure 6, the top sub-figure is the confusion matrix of the cVAE while the bottom one is of the proposed SDGZSL. The rows represent the groundtruth labels of the target test samples while the columns represent the predicted labels of the test samples. As unseen classes are hard to achieve high performance and can be usually misclassified into seen classes, we take the test samples from unseen classes to compare between the two settings. There are 10 unseen classes in AWA dataset, and almost all these classes in SDGZSL gain higher accuracy than cVAE. The test samples of unseen classes are usually misclassified into visually similar classes. Notably, in cVAE we can see that 41% of test samples from category "horse" are misclassified into "sheep", 31% from "sheep" to "cow", 35% from "rat" to "hamster". In contrast, our approach shows the ability to alleviate the problem by reducing the misclassification rate to 9%, 3%, and 35% for categories "horse", "sheep" and "rat", respectively. However, some extremely hard categories, *e.g.*, "seal" and "bat" can be easily misclassified into "walrus" and "rat", also fail in our proposed method. This will be investigated in our future work.

4.4.3 Hyper-Parameters

In the proposed SDGZSL, there are mainly four hyper-parameters that control the objective function, including the number of the disentangled feature dimension l , the

weight of *total correlation* term λ_1 , the weight of loss in the relation module λ_2 , and the weight of the discriminator loss λ_3 . To better understand the effect of the disentangling components, we report the sensitivity of the four hyper-parameters in Figure 7.

Varying the number of disentangled feature dimensions l . In our experiments, we set the dimension number of the semantic-consistent and the semantic-unrelated representations l and m as a same value. In Figure 7(a), we fix λ_1 , λ_2 and λ_3 and show the performance varies with the number of disentangled feature dimensions l . It can be seen that in most cases, the performance is sensitive to l and the optimal dimension number is around 312. Specifically, aPaY, AWA, CUB and FLO achieve the best result when $l = 128, 312, 312, 512$ respectively. Thus, the disentangled features have lower dimensions than the original CNN features that are 2048-dimensional, which will benefit the model in terms of the time complexity.

Varying the weight of relation module loss λ_1 . The relation module in our framework controls the visual-semantic connection for h_s . In Figure 7(b), we vary the weight of the relation module loss and compare the performance. The two coarse-grained datasets aPaY and AWA tend to fit to a low weight (1 and 0.5), whilst the fine-grained datasets CUB and FLO are optimal with a higher weight (both 5).

Varying the weight of TC λ_2 . We warm up the KL-divergence in cVAE together with our *total correlation* penalty gradually with increasing epochs. The warmup basis is set as 0.001, multiplying by the weight TC λ_1 as the TC increasing weight to linearly anneal it. Assume in epoch N^e , the final weight will be $0.001 * N^e * \lambda$. In Figure 7(c), we fix other hyper-parameters to see the trend of performance with respect to λ_2 . All 4 datasets have the best performance when $\lambda_2 = 1$. We can see that the performance is sensitive to the TC weight as a too high or too low weight is detrimental to the performance.

Varying the weight of discriminator loss λ_3 . The discriminator loss is used to optimize the discriminator Dis itself. We test different values of the weight of the discriminator loss in Figure 7(d), the optimal values for aPaY, AWA, CUB and FLO are 3, 3, 0.3, 1, respectively. It can be seen that the performance is not very sensitive to this value as the discriminator can converge in early epochs.

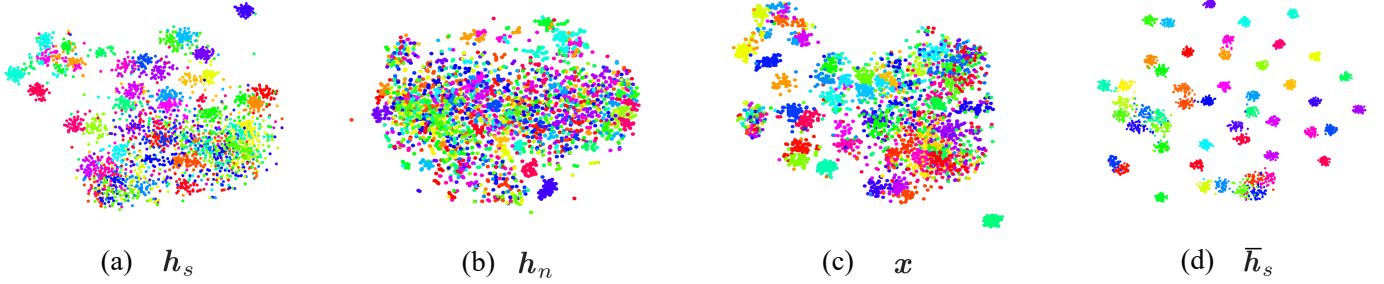


Fig. 8: t-SNE visualization of different representations of 50 unseen classes on CUB: (a) semantic-consistent representations h_s ; (b) semantic-unrelated representations h_n ; (c) original CNN visual features x ; (d) synthetic semantic-consistent representations \bar{h}_s .

TABLE 5: Conventional ZSL accuracy (%). The best results are formatted in bold.

Method	aPaY	AWA	CUB	FLO
ALE [3]	39.7	62.5	54.9	48.5
SJE [16]	31.7	61.9	54.0	53.4
ESZSL [20]	38.3	58.6	51.9	51.0
LFGAA [45]	-	68.1	67.6	-
DCN [46]	43.6	65.2	56.2	-
TCN [47]	43.6	65.2	56.2	-
GAZSL [22]	41.1	70.2	55.8	60.5
f-CLSWGAN [24]	40.5	65.3	57.3	69.6
cycle-CLSWGAN [49]	-	66.8	58.6	70.3
CADA-VAE [26]	-	64.0	60.4	-
f-VAEGAN-D2 [50]	-	71.1	61.0	67.7
DLFZRL [41]	46.7	70.3	61.8	-
TF-VAEGAN [29]	-	72.2	64.9	70.8
OCD-CVAE [51]	-	60.3	60.3	-
E-PGN [28]	-	73.4	72.4	85.7
SDGZSL	45.4	72.1	75.5	86.9

4.5 Conventional Zero-shot Learning Results

We aim to solve the generalized zero-shot learning problem in this work, but it is necessary to demonstrate that our approach can also achieve state-of-the-art performance on conventional zero-shot learning that only aims to classify unseen class samples over unseen classes. The results shown in Table 5 demonstrate the performance comparison between our proposed SDGZSL method and existing state-of-the-art models. It can be seen that our method outperforms all other methods on CUB and FLO datasets. Even if DLFZRL is slightly higher than our method on aPaY dataset, but we can surpass it on all other datasets. This is the same case for E-PGN on dataset AWA.

4.6 Visualization

4.6.1 Feature Visualization

To further validate the properties of the disentanglement, we visualize semantic-consistent representations h_s from x in Figure 8 (a), semantic-related representations h_n from x in (b), original visual features x in (c), and the generated semantic-consistent representations \bar{h}_s . Specifically, we adopt t-SNE to map the high-dimensional representations into a 2-dimensional plane. To make the visualization more intuitive, we choose all of 50 unseen classes from CUB

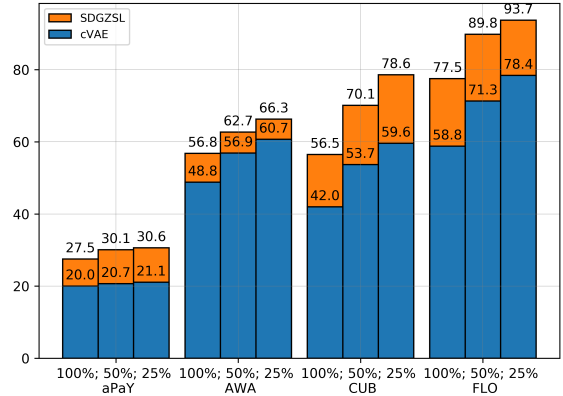


Fig. 9: Image retrieval results between cVAE and SDGZSL.

dataset that have enough classes to show the class-wise comparison. Clearly, h_s is much more discriminative than h_n . However, we can still see discriminative patterns from h_n as there are remaining discriminative features even if they are semantic-unrelated, e.g., characteristics that are not annotated in the attributes. But as the non-semantic discriminative features are not annotated in the attributes, it is intuitively impossible to transfer the semantic-visual relationship from seen classes to unseen classes. Figure 5 indicates the poor performance that the semantic-unrelated features h_n can only achieve on GZSL comparing to the semantic-consistent features h_s . Comparing Figure 8 (a) and (c), we can see that by semantic disentangling, h_s can be even more discriminative than the original visual features x . Figure 8 (d) shows the generated semantic-consistent representations \bar{h}_s can preserve the inter-class discrimination while keep the intra-class diversity.

4.6.2 Image Retrieval

We conduct the image retrieval task to illustrate the qualitative results of the proposed framework. Given the semantic embeddings of a specific class, we synthesize a certain number of semantic-consistent representations and compute the centroid point as a query to retrieval the nearest samples. To evaluate the retrieval performance, the standard metric of mean average precision (mAP) score is adopted. In Figure 9, we compare our proposed SDGZSL method with the base

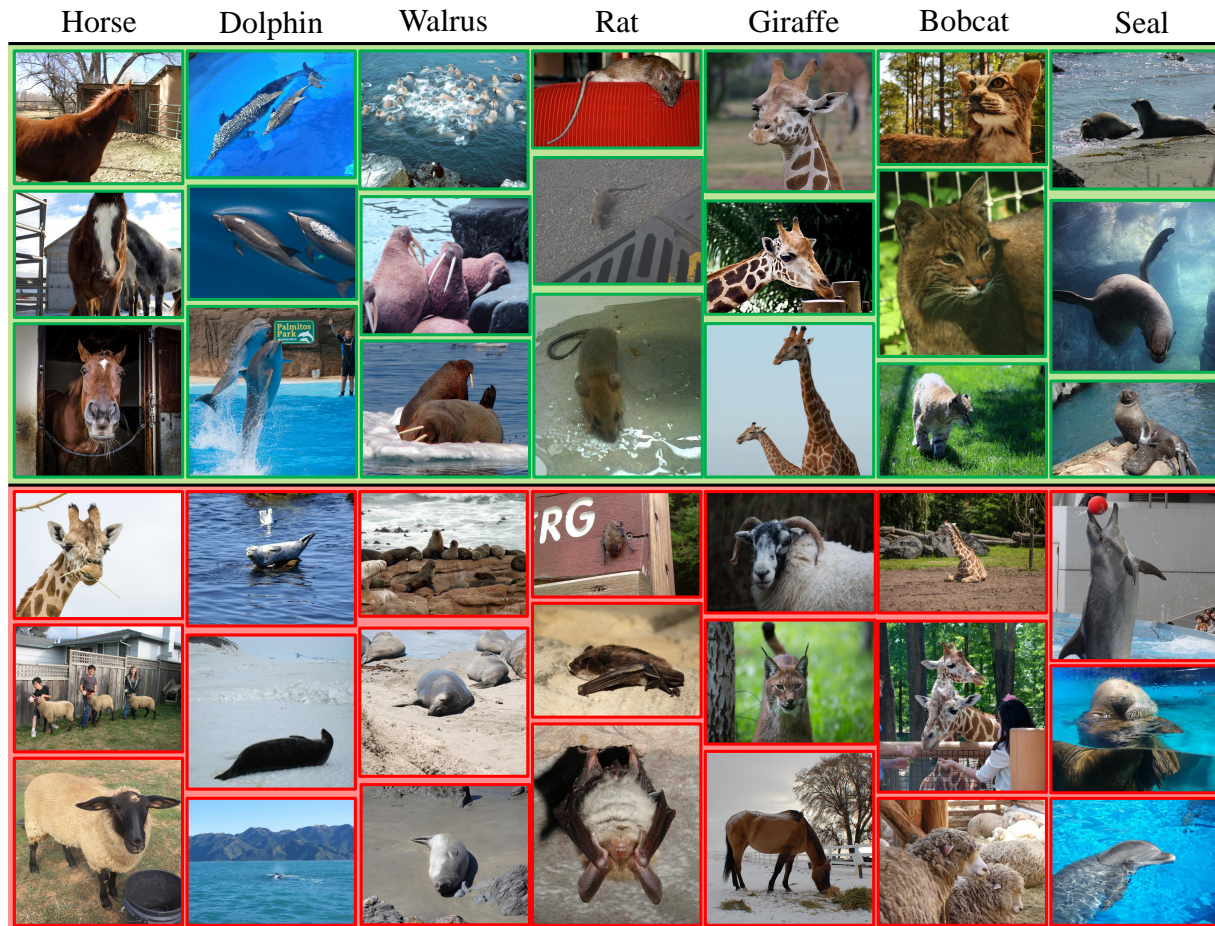


Fig. 10: Qualitative results of our approach on AwA, where 8 random unseen class labels are shown on top. The top-3 retrieved images are represented with green background and the top-3 retrieved false examples are given with red background.

generative model cVAE when retrieving 100%, 50%, and 25% of the images from all unseen classes on aPaY, AWA, CUB, and FLO datasets. It can be seen that the disentangling module built upon the cVAE model can significantly boost the retrieval performance among all settings. Figure 10 illustrates the retrieved examples on AWA dataset. The class name is given on top, following by the top-3 true positive retrieved images with green boxes and the top-3 false positive retrieved examples with red boxes. It can be seen that all the false positive images look very similar to the groundtruth examples. For example, the top-3 failed retrieved samples for the rat are all bats, as the two species have many visual patterns in common. Thus, the nearest neighbor-based retrieval may fail to distinguish the false positive cases. Such results demonstrate that the synthesized semantic-consistent representations are close to the samples of the same class in the semantic-consistent feature space.

5 CONCLUSION

In this paper, we propose a novel semantic disentangling approach for generalized zero-shot learning. Specifically, an image visual feature extracted pre-trained ResNet101, are further factorized into two independent representations

that are semantic-consistent and semantic-unrelated, respectively. In our approach, an encoder-decoder architecture is coupled with a relation module to learning the visual-semantic interaction. Further, we leverage the total correlation term to encourage the disentanglement between the two representations. The disentangling encoder-decoder model is incorporated into a conditional variational autoencoder (cVAE) and trained in an end-to-end manner. The overall framework is trained on the seen classes and generates semantic-consistent representations from attributes. The generation ability is transferred to the unseen classes and synthesize the missing visual samples. We evaluate our proposed method on five image classification and two action recognition datasets. Extensive experiments show that our approach consistently outperforms other state-of-the-arts.

REFERENCES

- [1] M. Norouzi, T. Mikolov, S. Bengio, Y. Singer, J. Shlens, A. Frome, G. S. Corrado, and J. Dean, "Zero-shot learning by convex combination of semantic embeddings," *arXiv preprint arXiv:1312.5650*, 2013.
- [2] Y. Xian, Z. Akata, G. Sharma, Q. Nguyen, M. Hein, and B. Schiele, "Latent embeddings for zero-shot classification," in *Proceedings of the IEEE Conference on Computer Vision and Pattern Recognition*, 2016, pp. 69–77.

- [3] Z. Akata, F. Perronnin, Z. Harchaoui, and C. Schmid, "Label-embedding for image classification," *IEEE transactions on pattern analysis and machine intelligence*, vol. 38, no. 7, pp. 1425–1438, 2015.
- [4] S. Changpinyo, W.-L. Chao, B. Gong, and F. Sha, "Synthesized classifiers for zero-shot learning," in *Proceedings of the IEEE Conference on Computer Vision and Pattern Recognition*, 2016, pp. 5327–5336.
- [5] E. Kodirov, T. Xiang, and S. Gong, "Semantic autoencoder for zero-shot learning," in *Proceedings of the IEEE Conference on Computer Vision and Pattern Recognition*, 2017, pp. 3174–3183.
- [6] C. H. Lampert, H. Nickisch, and S. Harmeling, "Attribute-based classification for zero-shot visual object categorization," *IEEE Transactions on Pattern Analysis and Machine Intelligence*, vol. 36, no. 3, pp. 453–465, 2013.
- [7] Z. Akata, F. Perronnin, Z. Harchaoui, and C. Schmid, "Label-embedding for attribute-based classification," in *Proceedings of the IEEE Conference on Computer Vision and Pattern Recognition*, 2013, pp. 819–826.
- [8] I. Goodfellow, J. Pouget-Abadie, M. Mirza, B. Xu, D. Warde-Farley, S. Ozair, A. Courville, and Y. Bengio, "Generative adversarial nets," in *Advances in neural information processing systems*, 2014, pp. 2672–2680.
- [9] D. P. Kingma and M. Welling, "Auto-encoding variational bayes," in *ICLR*, 2014.
- [10] F. Zhang and G. Shi, "Co-representation network for generalized zero-shot learning," in *International Conference on Machine Learning*, 2019, pp. 7434–7443.
- [11] K. He, X. Zhang, S. Ren, and J. Sun, "Deep residual learning for image recognition," in *Proceedings of the IEEE conference on computer vision and pattern recognition*, 2016, pp. 770–778.
- [12] A. Farhadi, I. Endres, D. Hoiem, and D. Forsyth, "Describing objects by their attributes," in *2009 IEEE Conference on Computer Vision and Pattern Recognition*. IEEE, 2009, pp. 1778–1785.
- [13] C. Wah, S. Branson, P. Welinder, P. Perona, and S. Belongie, "The caltech-ucsd birds-200-2011 dataset," 2011.
- [14] M.-E. Nilsback and A. Zisserman, "Automated flower classification over a large number of classes," in *2008 Sixth Indian Conference on Computer Vision, Graphics & Image Processing*. IEEE, 2008, pp. 722–729.
- [15] Z. Al-Halah, M. Tapaswi, and R. Stiefelhagen, "Recovering the missing link: Predicting class-attribute associations for unsupervised zero-shot learning," in *Proceedings of the IEEE Conference on Computer Vision and Pattern Recognition*, 2016, pp. 5975–5984.
- [16] Z. Akata, S. Reed, D. Walter, H. Lee, and B. Schiele, "Evaluation of output embeddings for fine-grained image classification," in *Proceedings of the IEEE conference on computer vision and pattern recognition*, 2015, pp. 2927–2936.
- [17] I. Tschantaridis, T. Joachims, T. Hofmann, and Y. Altun, "Large margin methods for structured and interdependent output variables," *Journal of machine learning research*, vol. 6, no. Sep, pp. 1453–1484, 2005.
- [18] A. Frome, G. S. Corrado, J. Shlens, S. Bengio, J. Dean, M. Ranzato, and T. Mikolov, "Devise: A deep visual-semantic embedding model," in *Advances in neural information processing systems*, 2013, pp. 2121–2129.
- [19] A. Krizhevsky, I. Sutskever, and G. E. Hinton, "Imagenet classification with deep convolutional neural networks," in *NIPS*, 2012.
- [20] B. Romera-Paredes and P. Torr, "An embarrassingly simple approach to zero-shot learning," in *International Conference on Machine Learning*, 2015, pp. 2152–2161.
- [21] Z. Chen, J. Li, Y. Luo, Z. Huang, and Y. Yang, "Canzsl: Cycle-consistent adversarial networks for zero-shot learning from natural language," in *The IEEE Winter Conference on Applications of Computer Vision*, 2020, pp. 874–883.
- [22] Y. Zhu, M. Elhoseiny, B. Liu, X. Peng, and A. Elgammal, "A generative adversarial approach for zero-shot learning from noisy texts," in *Proceedings of the IEEE Conference on Computer Vision and Pattern Recognition*, 2018, pp. 1004–1013.
- [23] M. Arjovsky, S. Chintala, and L. Bottou, "Wasserstein generative adversarial networks," in *International conference on machine learning*, 2017, pp. 214–223.
- [24] Y. Xian, T. Lorenz, B. Schiele, and Z. Akata, "Feature generating networks for zero-shot learning," in *Proceedings of the IEEE conference on computer vision and pattern recognition*, 2018, pp. 5542–5551.
- [25] H. Huang, C. Wang, P. S. Yu, and C.-D. Wang, "Generative dual adversarial network for generalized zero-shot learning," in *Proceedings of the IEEE Conference on Computer Vision and Pattern Recognition*, 2019, pp. 801–810.
- [26] E. Schonfeld, S. Ebrahimi, S. Sinha, T. Darrell, and Z. Akata, "Generalized zero-and few-shot learning via aligned variational autoencoders," in *Proceedings of the IEEE Conference on Computer Vision and Pattern Recognition*, 2019, pp. 8247–8255.
- [27] V. Kumar Verma, G. Arora, A. Mishra, and P. Rai, "Generalized zero-shot learning via synthesized examples," in *Proceedings of the IEEE conference on computer vision and pattern recognition*, 2018, pp. 4281–4289.
- [28] Y. Yu, Z. Ji, J. Han, and Z. Zhang, "Episode-based prototype generating network for zero-shot learning," in *Proceedings of the IEEE/CVF Conference on Computer Vision and Pattern Recognition*, 2020, pp. 14 035–14 044.
- [29] S. Narayan, A. Gupta, F. S. Khan, C. G. Snoek, and L. Shao, "Latent embedding feedback and discriminative features for zero-shot classification," *arXiv preprint arXiv:2003.07833*, 2020.
- [30] Y. Bengio, A. Courville, and P. Vincent, "Representation learning: A review and new perspectives," *IEEE transactions on pattern analysis and machine intelligence*, vol. 35, no. 8, pp. 1798–1828, 2013.
- [31] C. Eastwood and C. K. Williams, "A framework for the quantitative evaluation of disentangled representations," in *International Conference on Learning Representations*, 2018.
- [32] I. Higgins, L. Matthey, A. Pal, C. Burgess, X. Glorot, M. Botvinick, S. Mohamed, and A. Lerchner, "beta-vae: Learning basic visual concepts with a constrained variational framework," 2016.
- [33] R. T. Chen, X. Li, R. B. Grosse, and D. K. Duvenaud, "Isolating sources of disentanglement in variational autoencoders," in *Advances in Neural Information Processing Systems*, 2018, pp. 2610–2620.
- [34] S. Reed, K. Sohn, Y. Zhang, and H. Lee, "Learning to disentangle factors of variation with manifold interaction," in *International Conference on Machine Learning*, 2014, pp. 1431–1439.
- [35] M. F. Baln, A. Abid, and J. Zou, "Concrete autoencoders: Differentiable feature selection and reconstruction," in *International Conference on Machine Learning*, 2019, pp. 444–453.
- [36] D. Bouchacourt, R. Tomioka, and S. Nowozin, "Multi-level variational autoencoder: Learning disentangled representations from grouped observations," *arXiv preprint arXiv:1705.08841*, 2017.
- [37] S. Watanabe, "Information theoretical analysis of multivariate correlation," *IBM Journal of research and development*, vol. 4, no. 1, pp. 66–82, 1960.
- [38] H. Kim and A. Mnih, "Disentangling by factorising," *arXiv preprint arXiv:1802.05983*, 2018.
- [39] A. Abid, M. J. Zhang, V. K. Bagaria, and J. Zou, "Exploring patterns enriched in a dataset with contrastive principal component analysis," *Nature communications*, vol. 9, no. 1, pp. 1–7, 2018.
- [40] A.-H. Dirie, A. Abid, and J. Zou, "Contrastive multivariate singular spectrum analysis," in *2019 57th Annual Allerton Conference on Communication, Control, and Computing (Allerton)*. IEEE, 2019, pp. 1122–1127.
- [41] B. Tong, C. Wang, M. Klinkigt, Y. Kobayashi, and Y. Nonaka, "Hierarchical disentanglement of discriminative latent features for zero-shot learning," in *Proceedings of the IEEE Conference on Computer Vision and Pattern Recognition*, 2019, pp. 11 467–11 476.
- [42] K. Sohn, H. Lee, and X. Yan, "Learning structured output representation using deep conditional generative models," in *Advances in neural information processing systems*, 2015, pp. 3483–3491.
- [43] D. P. Kingma, S. Mohamed, D. Jimenez Rezende, and M. Welling, "Semi-supervised learning with deep generative models," *Advances in neural information processing systems*, vol. 27, pp. 3581–3589, 2014.
- [44] F. Sung, Y. Yang, L. Zhang, T. Xiang, P. H. Torr, and T. M. Hospedales, "Learning to compare: Relation network for few-shot learning," in *Proceedings of the IEEE Conference on Computer Vision and Pattern Recognition*, 2018, pp. 1199–1208.
- [45] Y. Liu, J. Guo, D. Cai, and X. He, "Attribute attention for semantic disambiguation in zero-shot learning," in *Proceedings of the IEEE International Conference on Computer Vision*, 2019, pp. 6698–6707.
- [46] S. Liu, M. Long, J. Wang, and M. I. Jordan, "Generalized zero-shot learning with deep calibration network," in *Advances in Neural Information Processing Systems*, 2018, pp. 2005–2015.
- [47] H. Jiang, R. Wang, S. Shan, and X. Chen, "Transferable contrastive network for generalized zero-shot learning," in *Proceedings of the IEEE International Conference on Computer Vision*, 2019, pp. 9765–9774.
- [48] S. Min, H. Yao, H. Xie, C. Wang, Z.-J. Zha, and Y. Zhang, "Domain-aware visual bias eliminating for generalized zero-shot learning," in *Proceedings of the IEEE/CVF Conference on Computer Vision and Pattern Recognition*, 2020, pp. 12 664–12 673.

- [49] R. Felix, V. B. Kumar, I. Reid, and G. Carneiro, "Multi-modal cycle-consistent generalized zero-shot learning," in *Proceedings of the European Conference on Computer Vision (ECCV)*, 2018, pp. 21–37.
- [50] Y. Xian, S. Sharma, B. Schiele, and Z. Akata, "f-vaegan-d2: A feature generating framework for any-shot learning," in *Proceedings of the IEEE Conference on Computer Vision and Pattern Recognition*, 2019, pp. 10275–10284.
- [51] R. Keshari, R. Singh, and M. Vatsa, "Generalized zero-shot learning via over-complete distribution," in *Proceedings of the IEEE/CVF Conference on Computer Vision and Pattern Recognition*, 2020, pp. 13300–13308.
- [52] S. Reed, Z. Akata, H. Lee, and B. Schiele, "Learning deep representations of fine-grained visual descriptions," in *Proceedings of the IEEE Conference on Computer Vision and Pattern Recognition*, 2016, pp. 49–58.
- [53] Y. Xian, C. H. Lampert, B. Schiele, and Z. Akata, "Zero-shot learning—a comprehensive evaluation of the good, the bad and the ugly," *IEEE transactions on pattern analysis and machine intelligence*, vol. 41, no. 9, pp. 2251–2265, 2018.
- [54] Z. Zhang and V. Saligrama, "Zero-shot learning via semantic similarity embedding," in *Proceedings of the IEEE international conference on computer vision*, 2015, pp. 4166–4174.